Valence-bond theory of linear Hubbard and Pariser-Parr-Pople models

Z. G. Soos and S. Ramasesha
Department of Chemistry, Princeton University, Princeton, New Jersey 08544
(Received 9 January 1984)

The ground and low-lying states of finite quantum-cell models with one state per site are obtained exactly through a real-space basis of valence-bond (VB) diagrams that explicitly conserve the total spin. Regular and alternating Hubbard and Pariser-Parr-Pople (PPP) chains and rings with N_e electrons on N (≤ 12) sites are extrapolated to infinite arrays. The ground-state energy and optical gap of regular $U=4|t|$ Hubbard chains agree with exact results, suggesting comparable accuracy for alternating Hubbard and PPP models, but differ from mean-field results. Molecular PPP parameters describe well the excitations of finite polyenes, odd polyene ions, linear cyanine dyes, and slightly overestimate the absorption peaks in polyacetylene $(CH)_x$. Molecular correlations contrast sharply with uncorrelated descriptions of topological solitons, which are modeled by regular polyene radicals and their ions for both wide and narrow alternation crossovers. Neutral solitons have no midgap absorption and negative spin densities, while the intensity of the in-gap excitation of charged solitons is not enhanced. The properties of correlated states in quantum-cell models with one valence state per site are discussed in the adiabatic limit for excited-state geometries and instabilities to dimerization.

I. INTRODUCTION

Quantum-cell models are defined by localized spins s_p or orbitals ϕ_p at sites $p=1,2,\ldots,N$. A single ϕ_p per site occurs in s-band solids, in Hubbard and related models, and in Pariser-Parr-Pople (PPP) models. The restriction to one electron per ϕ_p leads naturally to $s_p=\frac{1}{2}$ Heisenberg-spin models. Systems with N_e electrons on N sites, a single valence orbital ϕ_p per site, and spin-independent intersite interactions thus encompass many theoretical models in both physics and chemistry.[1] In addition to diverse applications, various approximate solutions have been proposed to augment the few exact results in one-dimensional arrays.

We present in this paper a real-space approach to cell models with a single ϕ_p per site and spin-independent interactions. As summarized in Sec. II, the use of valence-bond (VB) diagrams as basis states allows exact numerical solution for models with over 10^6 electronic configurations, while even 10^2 configurations for benzene were difficult for previous approaches based on molecular-orbital (MO) methods. The benzene ring of $N_e=N=6$ was independently solved by Heilmann and Lieb,[2] by Shiba and Pincus,[3] and by Schulten, Ohmine, and Karplus.[4] We find below low-lying states of $N_e=N=12$ Hubbard and PPP chains in C_2 symmetry using diagrammatic VB methods. Mazumdar and Dixit[5] have recently discussed the dimerization of $N_e=N=10$ Hubbard and extended Hubbard rings, also via VB methods, and summarize the related theoretical approaches.

For one-dimensional cell models, $N\sim 12$ sites suffices for accurate extrapolations to the infinite chain. Bonner and Fisher's famous[6] treatment of $s=\frac{1}{2}$ Heisenberg antiferromagnetic chains was restricted to $N\leq 12$. Lieb and Wu's exact results[7] for one-dimensional Hubbard models afford similar tests for extrapolation of the ground-state energy per site or of the optical gap, as discussed in Sec. III for different types of boundary conditions with common $N\rightarrow\infty$ limits. While finer points like critical exponents[8] require larger N, the electronic spectrum, transition moments, bond orders, spin densities, etc., may be extrapolated accurately for arbitrary spin-independent intersite interactions. PPP applications[9] to polyacetylene $(CH)_x$ in Secs. IV and V exploit $N\rightarrow\infty$ extrapolations for dimerized even chains and rings, for regular radicals representing neutral solitons, and for singlet ions describing charged solitons.

We choose orthonormal valence states ϕ_p and define fermion operators $a^\dagger_{p\sigma}, a_{p\sigma}$ for creating, annihilating an electron with spin σ in ϕ_p. The most general one-dimensional cell model with spin-independent interactions and nearest-neighbor t_p that conserve spin is

$$\mathcal{H}=\sum_{p,\sigma}[t_p(a^\dagger_{p\sigma}a_{p+1,\sigma}+a^\dagger_{p+1,\sigma}a_{p\sigma}) +\epsilon_p n_p+U_p n_p(n_p-1)/2] +\tfrac{1}{2}{\sum_{p,p'}}' V_{pp'}(n_p-z_p)(n_{p'}-z_{p'}) \; . \tag{1}$$

Here n_p is the number operator,

$$n_p=a^\dagger_{p\alpha}a_{p\alpha}+a^\dagger_{p\beta}a_{p\beta} \; . \tag{2}$$

The site energies ϵ_p, on-site correlations U_p, and intersite interactions $V_{pp'}$ are arbitrary in (1); their spin-independence is assured as coefficients of number operators. The usual case of Coulomb interactions requires the charge z_p at site p for empty ϕ_p. More distant transfers can also be handled via VB methods. Both $N_e=\Sigma n_p$ and the total spin S are conserved in (1) and the Lieb-Mattis theorem[10] holds for constant t_p. Even and odd N_e have

$S=0$ and $S=\frac{1}{2}$ ground states, respectively.

A real-space basis such as VB diagrams is off-diagonal for the t_p terms in (1), which alter the $\{n_p\}$, but is diagonal for all other contributions. Thus different ϵ_p, U_p, or $V_{pp'}$ merely change the diagonal elements, in sharp contrast to MO approaches where two-electron terms are off-diagonal. The t_p terms in (1) define the uncorrelated Hückel model. Adding U_p gives Hubbard models, while adding both U_p and $V_{pp'}$ leads to PPP models. The site energies ϵ_p are required for unlike atoms, as illustrated in Sec. V for cyanine dyes, or for donors and acceptors in solid charge-transfer complexes.[1] The general VB analysis of (1) is consequently independent of the parameter values of ϵ_p, U_p, or $V_{pp'}$. Spatial symmetries of chains or rings naturally allow reductions on forming symmetry-adapted linear combinations.

The direct solution of one-dimensional cell models has implications beyond understanding $(CH)_x$ or organic ion-radical solids. Like exact results, successful $N\rightarrow\infty$ extrapolations provide calibration for Hartree-Fock (HF), unrestricted HF, and other approximations that may be applied to far larger systems. The mean-field estimate of the optical gap of alternating Hubbard models, for example, needs revision. When several different self-consistent schemes are possible, the choice can be made by comparison with numerical results.

II. REAL-SPACE BASIS OF VB DIAGRAMS

The occupation numbers n_p and spins at each site are specified in any real-space basis. An N_e-fold product of operators $a^\dagger_{p\sigma}$ acting on the vacuum $|0\rangle$ yields an N_e-electron Slater determinant. Although S_z is readily conserved, linear combinations of Slater determinants are needed for eigenstates of S. Conventional VB diagrams, by contrast, explicitly pair spins in $n_p=1$ sites. The six-electron Kekulé, Dewar, and ionic VB diagrams in Fig. 1 are consequently singlets. Mazumdar and Soos[11] associate a normalized state $|k\rangle$ with each VB diagram by operating on $|0\rangle$ with $a^\dagger_{p\alpha}a^\dagger_{p\beta}$ for doubly filled ϕ_p, with $(a^\dagger_{p\alpha}a^\dagger_{q\beta}-a^\dagger_{p\beta}a^\dagger_{q\alpha})/\sqrt{2}$ for singlet-pairing of an electron in ϕ_p and another in ϕ_q, and with $a^\dagger_{p\alpha}a^\dagger_{q\alpha}$ for triplets in singly occupied sites at p and q. A few phase conventions suffice for generating $|k\rangle$ with arbitrary $S\leq N_e/2$ in terms of commuting, paired combinations of $a^\dagger_{p\sigma}$. Singlet pairing corresponds to covalent Heitler-London bonds that are denoted by lines in Fig. 1, while $S\geq 1$ involves an arrow connecting $2S$ sites and $S=\frac{1}{2}$ is handled separately. A diagram with m singlet lines represents a linear combination of 2^m Slater determinants. Linear independence and completeness is achieved by retaining[11] all diagrams without crossing lines or arrow on arranging the N sites at the vertices of a polygon.

The bit (binary digit) representation of VB diagrams introduced by Ramasesha and Soos[12,13] is the key for handling larger bases. Now $|k\rangle$ for an N-site diagram is written as a $2N$-digit binary number with bits $2p-2$, $2p-1$ associated with site $p=1,2,\ldots,N$, as shown in Fig. 1. Each benzene diagram becomes an integer I_k that is necessarily smaller than 2^{2N}. The code is 00 and 11 for empty and doubly occupied ϕ_p, respectively, while 10 and

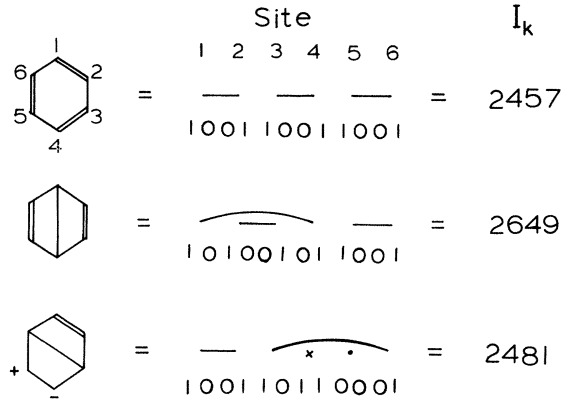

FIG. 1. Bit representation of π electrons in a Kekulé, Dewar, and ionic VB diagram of benzene.

01 represent the lower- and higher-numbered site of a singlet line, or the beginning and end of the line. Since lines do not cross in linearly independent $|k\rangle$, the binary code is unambiguous for $S=0$ and may readily be generalized to any $S\leq N_e/2$. Integers up to 2^{2N} are tested sequentially to generate P_s integers I_k representing linearly-independent VB diagrams with N_e electrons, N sites, and spin S. In addition to the compact notation, the increasing sequence I_k allows efficient tree searching. A similar procedure[13] based on a single bit per site may be used for $s_p=\frac{1}{2}$ sites, where only singly occupied ϕ_p occur.

Simple combinatorials for distributing N_e electrons on N sites always suffice for evaluating[11,13] the number P_s of linearly independent $|k\rangle$. Empty and doubly filled ϕ_p are nondegenerate singlets, while the spins of singly filled ϕ_p are coupled to form the total S. For example, even $N_e=2n$ and $N_e\leq N$ leads after some algebra to

$$P_s(2n,N)=\frac{2S+1}{N+1}\begin{bmatrix}N+1\\ n+1+S\end{bmatrix}\begin{bmatrix}N+1\\ n-S\end{bmatrix} \tag{3}$$

for $S=0,1,\ldots,n$ in terms of binomial coefficients. We usually require $S=0$ or 1 for even N_e and $S=\frac{1}{2}$ for odd N_e. The latter are found via the singlets of an expanded system with a singly occupied "phantom" at $N+1$ that does not participate in electron transfers under (1), but merely allows drawing nonintersecting lines connecting $n_p=1$ sites; (3) is again found, with n replaced by $N_e/2=n+\frac{1}{2}$. Some representative P_s are compared in Table I with the number of Slater determinants: $[(2n)!/n!n!]^2$ with $S_z=0$ and $N_e=N=2n$ and $[(2n+1)!/n!(n+1)!]^2$ with $S_z=\frac{1}{2}$ and $N_e=N=2n+1$ or with $S_z=0$ and $N=2n+1$, $N_e=N\pm 1$. The advantage[13] of the VB basis is even greater in spin problems based on purely covalent diagrams with all $n_p=1$.

Additional spatial or electron-hole symmetries require linear combinations of VB diagrams and reduce the $P_s\times P_s$ matrix of (1) for spin S. We suppose R_j to be one of $j=1,2,\ldots,G$ symmetry operators, with

$$[\mathscr{H},R_j]=0\,. \tag{4}$$

TABLE I. Dimensions of $S=0$ ($\frac{1}{2}$) subspaces for even (odd) N_e on N sites for VB diagrams and for the Slater determinants with $S_z=0$ (even) and $S_z=\frac{1}{2}$ (odd).

N_e/N	VB diagrams	Slater determinants
6/6	175	400
8/8	1764	4900
10/10	19 404	63 504
12/12	226 512	853 776
14/14	2 760 615	11 778 624
7/7	784	1225
9/9	8820	15 876
11/11	104 544	213 444
(6,8)/7	490	1225
(8,10)/9	5292	15 876
(10,12)/11	60 984	213 444

The coefficients of diagrams $R_j \mid k\rangle$ for $j=1,2,\ldots,G$ then differ at most by a phase factor. For larger N_e,N problems it is advantageous to store only

$$i_k=\min\{R_j \mid k\rangle\} . \tag{5}$$

The minimum integers i_k represent diagrams whose linear combination is fixed by symmetry. Unnormalized linear combinations suffice. Owing to highly symmetric diagrams similar to the Kekulé structure in Fig. 1, the exact subspaces are only approximately given by P_s/G, although this estimate is quite accurate for $N_e,N\sim 10$. We have $G=4$ for half-filled chains, $G=2$ for ionic chains, and $G=2N$ for half-filled regular rings.

We summarize next the representation of $\mathscr{H}$ in the VB basis. All terms of (1) other than the transfers t_p are diagonal and simply require the $\{n_p\}$ of i_k in (5), since all symmetry-related VB diagrams have identical ϵ_p, U_p, and $V_{pp'}$ contributions. The transfer terms interconnect VB diagrams

$$\sum_{p,\sigma} t_p(a^\dagger_{p\sigma}a_{p+1\sigma}+a^\dagger_{p+1\sigma}a_{p\sigma}) \mid k\rangle=\sum_j h_{kj} \mid j\rangle . \tag{6}$$

The completeness of the VB basis in the Hilbert space of one ϕ_p per site ensures that the matrix h is an exact representation of the transfer terms of (1). The fact that electron transfer occurs with spin conservation, as motivated physically by small spin-orbit coupling, ensures that $\mid j\rangle$ in (6) remains for the $\sim P_s/G$ linear combinations of diagrams for the chosen space and spin subspace. The $k\neq j$ coefficients h_{kj} have already been found for real transfers in ionic problems[11] and for virtual transfers[14] in Heisenberg exchange models. Furthermore, transfers between nonadjacent sites may systematically be represented[13] as products of nearest-neighbor transfers.

The nonorthogonality of the VB basis is not a major difficulty in the diagrammatic theory. The overlap matrix $S_{kk'}=\langle k \mid k'\rangle$ for singlets is real, symmetric, and found via Pauling's island-counting method,[15]

$$S_{kk'}=(-2)^{i-n+m} , \tag{7}$$

where $\mid k\rangle, \mid k'\rangle$ have identical $\{n_p\}, n-m$ singlet lines, and form $i\leq n-m$ disconnected cycles on superposing the two diagrams. Similar rules apply to diagrams with arbitrary spin. The elements h_{kj} in (6) form a nonsymmetric matrix $\underline{h}$ related[12] to the usual symmetric matrix representation by

$$\mathscr{H}=\underline{h}\,\underline{S}=\underline{S}\,\underline{h}^T . \tag{8}$$

The left eigenvector of $\underline{h}$ is the eigenstate ψ of $\mathscr{H}$,

$$\mid\psi\rangle=\sum_{k=1}^{P_s} c_k \mid k\rangle . \tag{9}$$

The coefficients c_k are chosen to normalize ψ, which explicitly involves a linear combination of the P_s diagrams $\mid k\rangle$ with fixed S, N_e, and N.

The matrix $\underline{h}$ is quite sparse, since N sites give $\sim N$ nearest-neighbor bonds and electron transfers to the right and left generate 0, 1, or 2 diagrams per bond. Each row in (6) has less than $2N$ nonvanishing elements for $\sim P_s/G$ symmetry-adapted basis vectors. The matrix $\mathscr{H}$ in (8) is far less sparse on multiplying by the overlap matrix. We note that MO bases involving one-electron orbitals, or N Fourier components in one-dimensional arrays, are even less sparse because two-electron terms in (1) generate $\sim N^2$ off-diagonal elements. The sparseness of the $\underline{h}$ matrix is a general feature of real-space bases with near-neighbor transfers, while spin conservation is achieved via the VB basis.

We have modified[13] the coordinate-relaxation procedure[16] for symmetric sparse matrices to give the lowest eigenstate of unsymmetric sparse matrices. Both the left and right trial vectors of h must be relaxed in the usual Rayleigh quotient. Deflation and further coordinate relaxation yield the second lowest eigenstate, thereby providing two states in each exact subspace with fixed S, spatial, and electron-hole symmetry. All computations were carried out on a Digital Equipment Corporation VAX-11/780 computer. The orthogonality of VB diagrams with unlike $\{n_p\}$ greatly simplifies[12] matrix elements over correlated states such as (9) for operators that do not change the total spin or the $\{n_p\}$. Transition moments and bond orders illustrate the former, spin densities and spin correlations the latter. We are not aware of previous procedures for matrix-elements evaluation in large configuration-interaction (CI) problems.

III. THE $U=4\mid t\mid$ HUBBARD MODEL

Hubbard models are restricted to on-site correlations. For $N_e=N$ electrons on equivalent sites, we take $\epsilon_p=V_{pp'}=0$ and $U_p=U$ in the general cell model (1). Bond alternation δ is defined as

$$t_p=t[1-\delta(-1)^p] \tag{10}$$

with $\delta=0.0$ for regular chains and $\delta>0$ for dimerized chains. We take $\mid t\mid=1$ as the unit of energy and $u=U/4\mid t\mid$ as the reduced on-site correlation. The most difficult and interesting case of $U=4\mid t\mid$ is studied for half-filled ($N_e=N$) Hubbard models.

Lieb and Wu[7] found exactly the ground-state energy per site $\epsilon(\delta,u)$ for regular Hubbard chains,

TABLE II. Ground-state energy per site, $\epsilon(\delta,1)/|t|$, of N-site Hubbard models with $U=4|t|$ and alternation δ. Rings of $4n$ and $4n+2$ form separate sequences.

	Regular ($\delta=0.0$)			Alternating ($\delta=0.07$)	
N	Chain	Chain ($N-1$)	Ring	Chain	Ring
6	−0.515 43	−0.483 50	−0.611 45	−0.546 13	−0.618 00
8	−0.529 48	−0.509 54	−0.575 44	−0.556 98	−0.586 94
10	−0.538 06	−0.526 93	−0.583 43	−0.563 52	−0.593 81
12	−0.543 85	−0.536 16	−0.576 70	−0.567 89	−0.589 57
∞		−0.573±0.005 (−0.573 73)[a]		−0.587±0.005	

[a]Exact, Ref. 7.

$$\epsilon(0,u)=-4\int_0^\infty \frac{J_0(\omega)J_1(\omega)}{\omega[1+\exp(2u\omega)]}d\omega\ . \tag{11}$$

The optical gap $E_g(\delta,u)$ for the lowest charge-transfer excitation at $\delta=0$ is[17]

$$E_g(0,u)=4u-4+8\int_0^\infty \frac{J_1(\omega)}{\omega[1+\exp(2u\omega)]}d\omega\ . \tag{12}$$

The corresponding results for the $\delta\to 1$ limit of decoupled Hubbard dimers are

$$\epsilon(1,u)=-(u^2+4)^{1/2}+u\ ,$$
$$E_g(1,u)=(u^2+4)^{1/2}\ . \tag{13}$$

The ground-state energy of alternating Hückel models was found by Longuet-Higgins and Salem[18]

$$\epsilon(\delta,0)=-\frac{4}{\pi}E[(1-\delta^2)^{1/2}]\ , \tag{14}$$

where E is the complete elliptic integral of the second kind. The Hückel gap is

$$\Delta E_g(\delta,0)=4\delta\ . \tag{15}$$

These exact results, all in units of $|t|$, are consistent with the physical expectations that a repulsive on-site interaction u makes $\epsilon(\delta,u)$ less negative while increasing alternation δ makes $\epsilon(\delta,u)$ more negative. The optical gap $E_g(\delta,u)$ increases with both u and δ.

Table II contains $\epsilon(\delta,u)$ results for chains and rings up to $N_e=N=12$. Boundary conditions must become irrelevant as $N\to\infty$. Regular Hückel rings of $4n$ sites have orbitally degenerate ground states and $\epsilon(0,0,4n)$ converges strictly from above, while $4n+2$ regular Hückel rings have nondegenerate $\epsilon(0,0,4n+2)$ that converge strictly from below. These trends persist in Table II at $U=4|t|$ and give separate sequences for $4n$ and $4n+2$ rings. The weak n dependence of $\epsilon(0,1,4n)$ must eventually reverse in view of the exact result (11). As found in spin systems[6,13] and shown in Fig. 2, $\epsilon(\delta,u)$ converge approximately as N^{-2} and N^{-1}, respectively, for rings and chains. The functional dependence on N is, however, not known *a priori*. Extrapolations of independent sequences are consequently more accurate,[13] especially when convergence is from both above and below, and also suggest the uncertainty at $N\to\infty$. The present $\epsilon(\delta,1)$ results are good to better than $\pm5\times10^{-3}$ at either $\delta=0.0$ or 0.07.

The optical gap $E_g(\delta,1)$ is extrapolated as N^{-1} in Fig. 3 for even chains and $4n,4n+2$ rings. Numerical results are collected in Table III. All regular $4n$ Hückel rings have vanishing gap, while $E_g(0,0,4n+2)$ decreases[19] as N^{-1}. These features will be more evident in Sec. III for PPP models with standard parameters. The $U=4|t|$ gaps in Fig. 3 decrease for both chains and rings and consequently provide less accurate extrapolations; the strongest dependence is found as expected in $4n+2$ rings and will require $N=14$ results. The extrapolated $E_g(0,1)=1.20\pm0.10$ for chains and $4n$ rings is within 10% of the exact result, 1.2867, from (12).

The mean-field result[20] for the optical gap is

$$E_{\rm mf}(\delta,u)=[E_g^2(0,u)+(4\delta)^2]^{1/2}\ . \tag{16}$$

Quite typically, the squares of the $u=0$ result (15) and the $\delta=0$ result (12) are combined. Numerical results for alternating Heisenberg spin chains, whose smaller basis allows $N=20$ chains and rings, indicate[8] that the gap opens

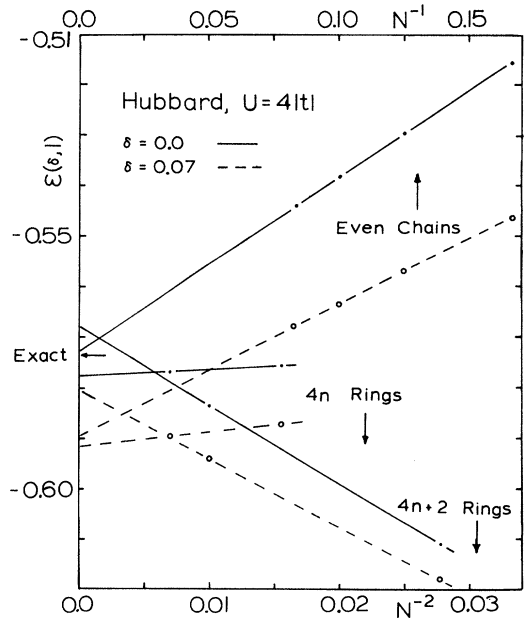

FIG. 2. Ground-state energy per site ϵ in units of $|t|$ vs N^{-1} for chains and N^{-2} for rings in regular ($\delta=0.0$) and alternating ($\delta=0.07$) Hubbard models with $U=4|t|$; the exact $\delta=0.0$ result is from Ref. 7.

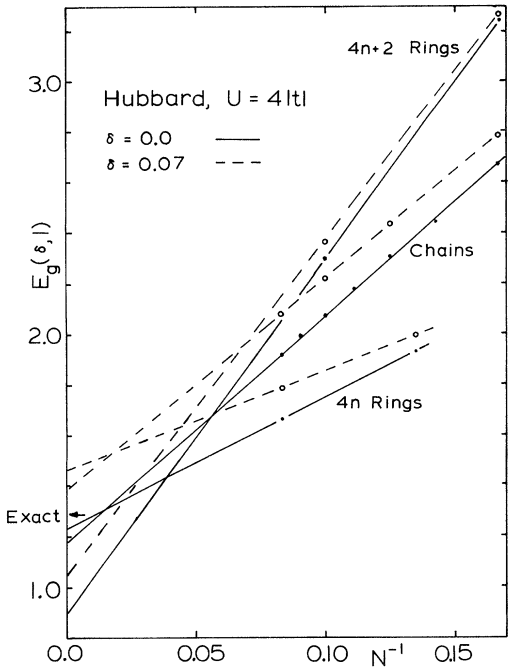

FIG. 3. Optical gap E_g in units of $|t|$ vs N^{-1} for regular and alternating Hubbard models with $U=4|t|$; the exact $\delta=0.0$ result is from Ref. 17.

as δ^{ν} with $\nu=0.9\pm0.1$. The less complete results for $N\leq 12$ in Table II are in clear disagreement with (16), since $\delta=0.07$ produces a 0.20 increase at $u=1$, while (16) predicts an increase of less than 0.03. The critical exponent ν is more difficult to estimate. The point here is that $E_g(\delta,u)$ increases with δ far more rapidly than (16).

Any alternation $\delta>0$ may be converted to dimerization $x=\delta/\alpha$ by introducing a linear electron-phonon coupling α. A harmonic restoring potential per site, in units of $|t|$,

$$c\delta^2/2=cx^2/(2|t|\alpha^2) \tag{17}$$

favors the regular lattice. Longuet-Higgins and Salem demonstrated[18] the instability of linear Hückel models to dimerization. The electronic energy change per site in (14) for small δ is

$$\Delta\epsilon(\delta,0)=\epsilon(\delta,0)-\epsilon(0,0)\sim\delta^2\ln|\delta|\ , \tag{18}$$

which clearly exceeds any finite restoring potential in (17).

The instability of Hubbard chains has subsequently been studied by several groups, as summarized by Mazumdar and Dixit.[5] Mean-field theories tend to give decreasing dimerization with increasing u, while more exact treatments suggest that $u<1$ enhances the dimerization. Mazumdar and Dixit[5] combine general topological arguments for $4n+2$ rings with numerical results for 6- and 10-site rings to obtain enhanced dimerization up to $u\sim1$. The Jahn-Teller distortion of $4n$-site Hückel rings make these unsuitable for their analysis, although this distinction must disappear as $n\rightarrow\infty$.

In view of the difficulties of finding critical exponents for $\Delta\epsilon(\delta,u)$ in (18), we focus on fixed δ. The constant c in (17) may always be chosen to give a minimum at δ for a Hückel chain, whose electronic $|\Delta\epsilon(\delta,0)|$ is given in (18). We have increased or decreased dimerization, respectively, whenever $|\Delta\epsilon(\delta,u)|$ is larger or smaller than the $u=0$ value. The main advantage of this approach is that infinite chains are compared directly. The stabilization $|\Delta\epsilon(\delta,u)|$ is shown in Fig. 4 for even chains and $4n,4n+2$ rings at $\delta=0.07$ and $u=1$. All three extrapolations exceed the Hückel value and point to increased dimerization at $u=1$ and $\delta=0.07$, in agreement with recent results[5] beyond the mean-field limit. But the reverse holds for large δ, when $u=1$ decreases the dimerization relative to $u=0$.

The physically unrealistic but exactly soluble case of linear electron-phonon coupling for large distortions $\delta\rightarrow1$ is instructive. Now (13) and (11) yield $|\Delta\epsilon(1,u)|$, which is always smaller than the Hückel value, $2-4/\pi$. Thus any $u>0$ decreases the dimerization at $\delta=1$ and $u=1$ increases dimerization relative to Hückel chains only for slightly dimerized chains which, however, are realized experimentally. The interplay of u and δ in Hubbard chains is complicated and requires accurate $\epsilon(\delta,u)$ values. The main features could be obtained from extrapolations based on $N\leq12$ rings and chains, but the procedure is inevitably tedious. In addition, larger N and/or better extrapolations should be considered before computing chains and rings at many values of u and δ.

IV. EVEN PPP CHAINS AND RINGS

Finite even polyenes have alternating double and single carbon-carbon bonds in the ground state, as sketched in Fig. 5(a). Typical estimates[19] of the transfer integral $|t|$ in (10) range from -2.2 to -2.6 eV; we adopt the standard values[21] $|t|=-2.40$ eV and alternation $\delta=0.07$ for nominally double and single $C-C$ bonds of length $r_d=1.35$ and 1.45 Å, respectively. Unless otherwise stated, we take the idealized all-*trans* geometry with 120° an-

TABLE III. Optical gap $E_g/|t|$ of N-site Hubbard model with $U=4|t|$ and alternation δ. Rings of $4n$ and $4n+2$ form separate sequences.

	Regular ($\delta=0.0$)			Alternating ($\delta=0.07$)	
N	Chain	Chain ($N-1$)	Ring	Chain	Ring
6	2.670	2.926	3.249	2.784	3.275
8	2.306	2.442	1.931	2.440	2.011
10	2.076	2.177	2.296	2.227	2.369
12	1.920	1.991	1.667	2.085	1.789
∞		1.20±0.10 (1.2867)[a]		1.40±0.10	

[a]Exact, Ref. 17.

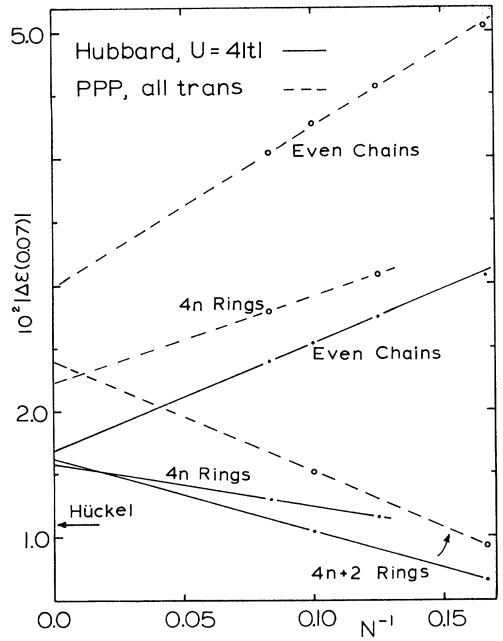

FIG. 4. Electronic energy gain per site, $|\Delta\epsilon|/|t|$ vs N^{-1} for alternation $\delta=0.07$ in $U=4|t|$ Hubbard models and in PPP models with standard molecular parameters; the exact Hückel result is given by Eqs. (18) and (14).

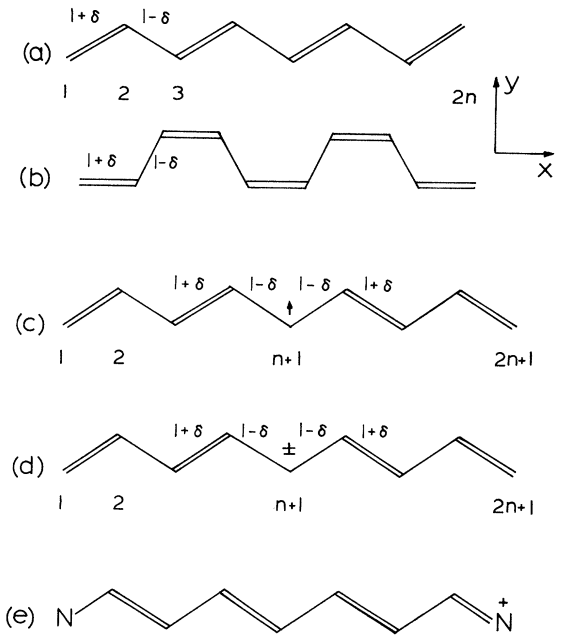

FIG. 5. Idealized ground-state geometry of conjugated π-electron systems with 120° angles: (a) $2n$-site all-*trans* polyene, (b) *cis-transoid* even polyene, (c) polyene radical with central alternation crossover, (d) ions of odd polyenes with a central crossover, and (e) linear cyanine dye.

gles in Fig. 5(a). Cyclic boundary conditions in the x-z plane leave the polyene width along y undisturbed. The same bond lengths and angles are used for the *cis-transoid* geometry in Fig. 5(b).

The parametrization of PPP models is a separate topic.[19,21,22] We adopt standard molecular values, with $U=11.26$ eV for C^- sites from gas-phase ionization and electron affinity data. Intersite Coulomb interactions $V_{pp'}$ between charged C^+ or C^- sites in the cell model (1) go as $\pm e^2/r_{pp'}$ for distant sites. They are interpolated to U according to the Ohno formula,[23]

$$V_{pp'}=U(1+0.6117r_{pp'}^2)^{-1/2}\ . \tag{19}$$

The geometry and U thus fix all intersite interactions. These gas-phase values may eventually require corrections in solids, for example, by considering dielectric and polarization effects. Finally, we set $\epsilon_p=0$ for carbon atoms in polyenes, thereby defining a convenient reference energy.

The preceding remarks fix all the parameters in the cell model (1). The molecular correlations $V_{pp'}$ in (19) and $|t|=-2.40$ eV in (10) are denoted collectively as u' and kept without change for consistent comparison at alternations $\delta=0.0$ and $\delta=0.07$. As indicated in Table IV, standard molecular parameters correctly place the two-photon 2^1A_g state below the dipole-allowed 1^1B_u excitation in polyenes with 4, 5, and 6 double bonds. This reversal from the HF order has been extensively discussed[24,1] as evidence for highly correlated states. The agreement in Table IV may be improved by ~ 0.3 eV on relaxing the excited-state geometry,[25] as determined by its π-bond orders. We have also noted in Table IV excitations[26] of anions of odd polyenes, whose geometry is essentially regular.

To examine infinite alternating chains in $(CH)_x$, we begin with the ground-state energy $\epsilon(\delta,u')$ per site of even PPP chains and rings. The results in Table V are extrapo-

TABLE IV. Optical gap E_g and two-photon excitation energy of gas-phase polyenes with N carbons, $N_e\pi$ electrons, and alternation δ. The PPP results are for all-*trans* geometry and molecular parameters.

			E_g (eV)		2^1A_g (eV)	
N	N_e	δ	PPP	Expt.	PPP	Expt.
Molecules[a]						
8	8	0.07	4.561	4.40	3.775	3.59
10	10	0.07	4.234	4.02	3.404	3.10
12	12	0.07	4.001	3.65		2.73
Ions[b]						
5	6,4	0.0	3.456	3.42		
7	8,6	0.0	2.799	2.88		

[a]Expt, Table II, Ref. 24.
[b]Expt, Ref. 26.

TABLE V. Ground-state energy per site $\epsilon(\delta,u')$ in eV of N-site PPP models with molecular parameters and alternation δ. Rings of $4n$ and $4n+2$ form separate sequences.

	All-*trans* (δ=0.0)		All-*trans* (δ=0.07)		*cis-transoid* (δ=0.07)	
N	Chain	Ring	Chain	Ring	Chain	Ring
6	−1.9519	−2.3243	−2.0730	−2.3467	−2.0735	−2.4233
8	−1.9957	−2.0990	−2.1054	−2.1730	−2.1063	−2.1821
10	−2.0228	−2.1995	−2.1250	−2.2358	−2.1267	−2.2766
12	−2.0413	−2.1315	−2.1382	−2.1987	−2.1395	−2.2029
∞	−2.14±0.02		−2.20±0.02		−2.20±0.02	

lated in Fig. 6 as N^{-2} for rings and as N^{-1} for chains. Convergence from above and below is again found, as in $U=4|t|$ Hubbard models in Fig. 2, and the accuracy is ±0.02 eV for both $\delta=0.0$ and 0.07. The *cis-transoid* results in Table V extrapolate within experimental error to the *trans* value.

The dipole-allowed 1^1B_u excitation defines the optical gaps E_g in Table VI for even PPP chains and rings. As shown in Fig. 7, $E_g(\delta,u',4n)$ converges from below, which is a remnant of the vanishing gap in regular $4n$ Hückel rings. We also note that E_g for even and odd regular chains in Fig. 8 falls on the same line, in sharp contrast with alternating odd Hückel chains[19] with a midgap absorption. We return to this point in Sec. V.

The extrapolated gap[9] E_g of 2.8±0.2 eV for infinite PPP chains with alternation 0.07 in Fig. 8 is a single-strand or gas-phase result. The 0.0 absorption for finite polyenes in solution or in matrices is red shifted[27] by ~0.5 eV depending on the medium's polarizability. The absorption maxima[28] of *cis* and *trans* $(CH)_x$ indicated in Fig. 7 are consequently in fair agreement with theory and suggest at most small reductions in the correlations. The optical gaps for conjugated polymers estimated by MO methods[29] are several volts higher, even for self-consistent

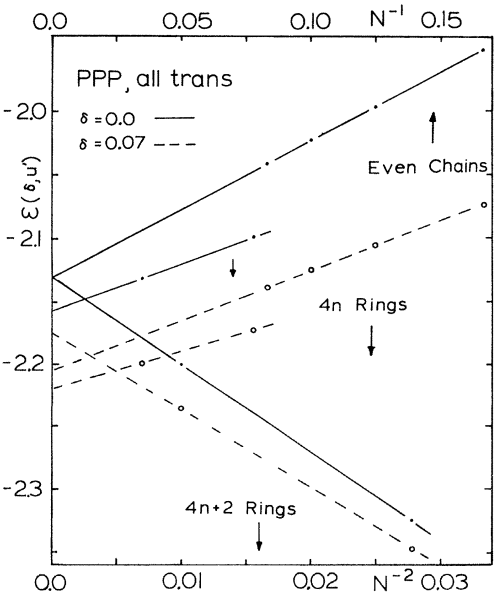

FIG. 6. Ground-state energy per site ϵ vs N^{-1} for chains and N^{-2} for rings in regular (δ=0.0) and alternating (δ=0.07) PPP models with correlations given in Eq. (19).

calculations. Direct solution of the PPP cell model (1) is thus required for accurate excitation energies in both finite and infinite polyenes.

The $\epsilon(\delta,u')$ and $E_g(\delta,u')$ entries for *cis-transoid* $(CH)_x$ in Tables V and VI are, contrary to experiment, consistently below the *trans* values. PPP theory favors the *cis* isomer because its more compact geometry slightly stabilizes highly-ionic excited VB diagrams and thus enhances their CI with low-lying, largely covalent states. The physically important nonbonded H-H repulsions that destabilize *cis* relative to *trans*, are not included in the π-electron model (1). All-electron MO treatments[29] without CI often give good ground-state geometries and relative stabilities, while model Hamiltonians such as (1) focus on excitation energies.

The instability of PPP models at $\delta=0.07$ may be compared to the Hückel result, as discussed above for $U=4|t|$ Hubbard models. The convergence of $\Delta\epsilon(0.07,u')$ in (18) for even chains and $4n+2$ PPP rings is less accurate, as shown in Fig. 4, no doubt because long-range Coulomb interactions increase the sensitivity to different boundary conditions. The intercept in Fig. 4 is 2.6±0.4, as compared to 1.6±0.1 for the $U=4|t|$ Hubbard model and 1.1077 for the Hückel model. The PPP model with standard parameters is consequently far more prone to dimerization. The harmonic restoring potential in (17), for example, more than doubles over the Hückel value to maintain alternation $\delta=0.07$.

The covalent 2^1A_g states below E_g in Table IV, as well as even lower[12] 1^3B_u triplets, may be characterized from the corresponding excitations of Hubbard and Heisenberg chains. The infinite regular half-filled Hubbard chain has[17] a band of singlet and triplet excitons with vanishing gaps at long wavelength ($k\to 0$). Regular Heisenberg antiferromagnetic chains also have vanishing gaps for the lowest triplet and singlet spin waves. Gaps for both open up for $\delta>0$. We consequently anticipate covalent gaps for both triplet spin excitons derived from 1^3B_u and singlet spin excitons derived from 2^1A_g in alternating Hubbard and PPP chains. The covalent gaps vanish in regular chains and have vanishing oscillator strength for dipole transitions at any δ.

V. ODD PPP SEGMENTS: SOLITONS AND CYANINE DYES

Neutral polyene radicals in Fig. 5(c) have $S=\frac{1}{2}$ ground states and odd $N_e=N$; their ions in Fig. 5(d) have singlet ground states. Infinite odd segments contain an alternation crossover, or a topological soliton. Su, Schrieffer,

TABLE VI. Optical gap E_g in eV of N-site PPP models with molecular parameters and alternation δ. Rings of $4n$ and $4n+2$ form separate sequences.

	All-*trans* (δ=0.0)		All-*trans* (δ=0.07)		*cis-transoid* (δ=0.07)	
N	Chain	Ring	Chain	Ring	Chain	Ring
6	4.693	6.214	5.046	6.230	5.016	5.521
8	4.171	1.624	4.561	2.164	4.508	1.971
10	3.812	4.154	4.234	4.301	4.162	3.845
12	3.552	1.712	4.001	2.383	3.914	2.144
∞	2.4±0.2		2.8±0.2		2.8±0.2	

and Heeger[30] (SSH) predict a crossover of $2\xi \sim 15$ in uncorrelated (Hückel) chains with linear electron-phonon coupling and optical gap $4\,|\,t\,|\,\delta \sim 1.4$ eV. These Hückel-based results are significantly altered by correlations.[31,32,9]

To extrapolate consistently, we consider two limiting geometries. Since δ vanishes near the center of crossover, any $N < 2\xi \sim 15$ segment may be taken as regular (δ=0.0) to mimic a wide domain wall. Conversely, a sharp ($\xi \to 0$) crossover immediately reverts to alternation δ about a central spin in $4n+1$ segments and a central allyl in $4n-1$ segments that begin and end with double bonds. The two bonds of the allyl are intermediate at $|\,t\,|$, just as in benzene, with r=1.40 Å. The emergence of separate $4n+1, 4n-1$ sequences is better illustrated by spin solitons[13] in odd-length Heisenberg antiferromagnetic chains, where $N \leq 19$ is readily accessible.

We retain the all-*trans* geometry in Fig. 5 and standard PPP parameters for the optical gaps of regular radicals in Table VII, which fall on the same line as regular even polyenes in Fig. 7. By contrast, $2n+1$ site Hückel models with $\delta > 0$ have a nonbonding, singly occupied MO precisely at the gap center for any $\{t_p\}$ according to the pairing theorem.[19] Excitations at $E_g/2$ then involve either exciting the nonbonding electron to the bottom of the conduction band or exciting an electron from the top of the valence band into the nonbonding state. Correlations[31] split the degeneracy and, within cell models (1) with equivalent sites and $N_e = N$, all the oscillator strength goes into the upper state. The covalent gap in Fig. 8 is the lower state that becomes degenerate with the upper state at $E_g/2$ in Hückel theory. The $E_g/2$ excitations of charged solitons, with empty or doubly filled nonbonding MO, are nondegenerate and less sensitive to correlations.[31] Sharp domain walls increase slightly ($<$0.2 eV) the absorption of neutral radicals. Weinberger *et al.*[33] have recently confirmed that paramagnetic states in $(CH)_x$ do not absorb in the midgap region, while charged states do.

Optical gaps for odd polyene ions, or charged solitons, are given in Table VII for both regular chains and sharp domain walls. The δ=0.0 data are plotted against N^{-1} in Fig 8. In PPP models with common ϵ_p, U_p parameters at all sites, electron-hole symmetry gives identical electronic excitations for $N_e = N \pm 1$. Positive and negative solitons may consequently be treated together. The exactly soluble[34] regular Hubbard model with $N_e \neq N$ has vanishing

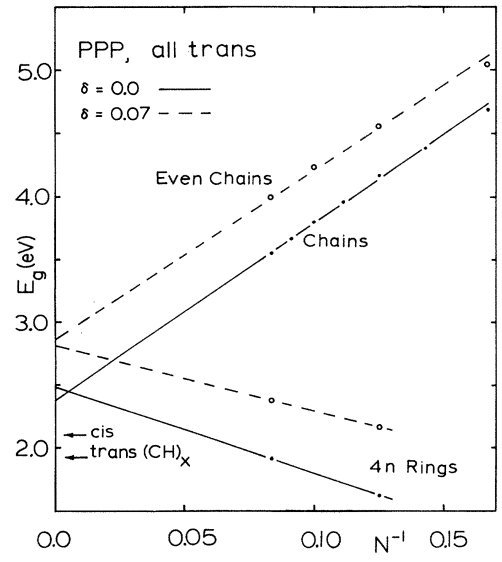

FIG. 7. Optical gap E_g vs N^{-1} of regular and alternating PPP models with molecular correlations.

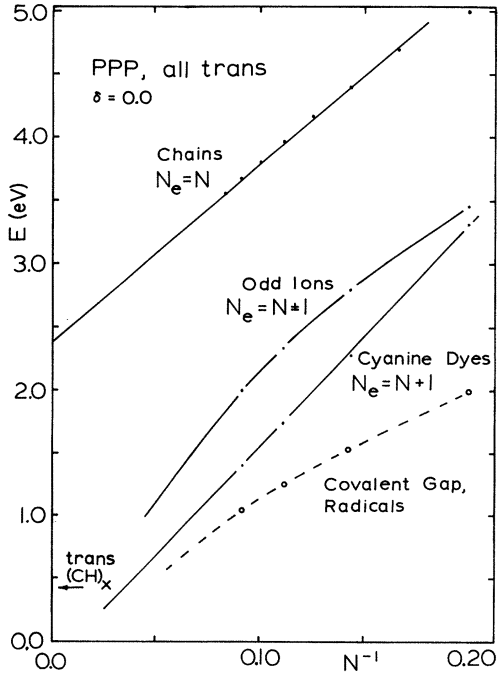

FIG. 8. Optical gaps vs N^{-1} of regular PPP chains with molecular correlations, ions of odd segments representing charged solitons and linear cyanine dyes; the covalent gap of radicals is dipole forbidden.

TABLE VII. Optical gap E_g in eV for N-site all-*trans* polyene radicals, their ions, and cyanine dyes, with standard PPP parameters and either regular ($\delta=0.0$) geometry or alternation $\delta=0.07$ and a sharp central domain wall ($\xi=0$).

	Radicals ($N_e=N$)	Odd ions ($N_e=N\pm1$)		Cyanines ($N_e=N+1$)
N	$\delta=0.0$	$\delta=0.0,\xi\to\infty$	$\delta=0.7,\xi=0$	$\delta=0.0$
5	5.009	3.456	3.493	3.075
7	4.389	2.799	2.875	2.128
9	3.969	2.343	2.429	1.547
11	3.669	2.009	2.116	1.221

E_g, and this expectation also applies to partly filled PPP models. The extrapolation for odd ions in Fig. 8 is consistent with a vanishing gap, given the downward curvature, and the dipole-allowed excitations are certainly below $E_g/2$.

A sharp central domain wall increases E_g for charged solitons in Table VII, with the greatest change at large N. Extrapolations are not sufficiently accurate, however, to go beyond such qualitative results as $E_g<0.4$ eV as $N\to\infty$. The more realistic picture of a finite crossover of $\sim 2\xi$ sites is intermediate between the $\delta=0.0$ ($\xi\to\infty$) and $\xi=0$ limits. The photogenerated *trans* $(CH)_x$ state[35] at 0.43 eV indicated in Fig. 8 is associated with charged solitons. The latter are ions of odd polyenes in the model[9] of fixed finite segments defined by crosslinks, chain ends, or defects.

The qualitatively different length dependence of π-π^* excitations of polyenes and cyanine dyes has long been recognized.[22,19] It turns out to be largely a correlation effect in half-filled ($N=N_e$) even polyenes and linear cyanine dyes or odd ions with $N_e=N+1$. Strong correlations provide the simplest physical picture for the difference. When the most covalent VB diagrams dominate, an electron-hole pair at $E_g\sim U-V_1$ is the lowest dipole-allowed excitation in half-filled bands. For $N_e=N+1$, on the other hand, the ground state already contains linear combinations of diagrams with one ion among N sites. Low-energy E_g excitations do not require additional ions, but merely change the linear combination and occur at vanishing energy in regular infinite arrays.

The chemical formula of a type-I cyanine dye[22] is $R_2N-(CH=CH)_n-C=NR_2$, as sketched in Fig. 5(e). The π system has odd N, with terminal nitrogens each providing two electrons and thus requiring $z_1=z_N=2$ in the cell model (1). Then $N_e=N+1$ is even and the ground state is a singlet. Typical molecular parameters[36,25] for nitrogen are $\epsilon_1=\epsilon_N=-18.43$ eV relative to $\epsilon_p=0$ at carbons, again from gas-phase atomic data, and $U_1=U_N=15$ eV, to reflect the more compact $2p_z$ orbital relative to $U=11.26$ eV for carbon. The Ohno[23] formula (19) now reads

$$V_{pp'}=\left[\left[\frac{2}{U_p+U_{p'}}\right]^2+\left[\frac{r_{pp'}}{14.397}\right]^2\right]^{-1/2}, \tag{20}$$

with $V_{pp'}$ in eV and $r_{pp'}$ in Å. We retain regular all-*trans* segments with $|t|=-2.40$ eV. Some alternation occurs in longer cyanines and the C-N transfer is somewhat higher. Different t_p may readily be incorporated since the point-group symmetry is not reduced.

The resulting E_g in Table VII and Fig. 8 vanish more linearly with N^{-1} than the isoelectronic odd anions. The stable even polyenes have alternation $\delta\sim 0.07$ and higher E_g given in Table VI and Fig. 7; the lower E_g for regular PPP chains in Fig. 8 also remains finite as $N\to\infty$. We have consequently illustrated how PPP parameters are changed for different atoms and shown that quite different ϵ_p, U_p, and $V_{pp'}$ values in (1) lead to vanishing E_g in regular infinite chains with $N_e=N\pm1$.

VI. PROPERTIES OF CORRELATED STATES

The restriction to one ϕ_p per site in the general cell model (1) yields a large but finite basis. VB methods then provide exact results for models that conserve S. In addition to eigenvalues, correlated states such as (9) may be used to evaluate matrix elements of interest.[12] In all cases, ψ is a linear combination of $\sim P_s$ diagrams with fixed S. The familiar orbital picture is lost, however, and the unfamiliarity of correlated states remains a problem.

We discuss first some exact properties of cell models (1) with one ϕ_p per site. The Lieb-Mattis theorem,[10] that the ground state has the lowest possible S, applies to a one-dimensional array with constant nearest-neighbor $t_p=t$, $\epsilon_p=0$ and arbitrary spin-independent potential $V(\ldots,n_p,\ldots)$. We expect and find $S=0$ ground states for even N_e and $S=\frac{1}{2}$ for odd N_e in finite chains.

The case $N_e=2N$ is trivially identical to VB and MO theory, since doubly occupying all ϕ_p gives a nondegenerate closed shell. Special properties also occur for $N_e=N$, the half-filled case, as discussed[19] extensively for Hückel models as the pairing theorem and Pariser's alternancy symmetry.[37,38] $N_e=N$ results for the cell model (1) involve the electron-hole (*eh*) symmetry.[37–39] The *eh* operator commutes[2,39] with $\mathscr{H}$ for equivalent sites (ϵ_p, U_p, and $z_p=1$, all independent of p) and $N_e=N$. It behaves like a symmetry operator R_j in (4) and gives for each eigenstate of (1),

$$n_p=1 \quad (p=1,2,\ldots,N), \tag{21}$$

whenever $[R_{eh},\mathscr{H}]=0$. This exact result precludes a charge-density-wave (CDW) ground state in cell models with *eh* symmetry.

The *eh* operator[29] simply interchanges empty and doubly occupied ϕ_p, which occur with equal frequency in each diagram $|k\rangle$ for $N_e=N$, and multiplies the new diagram $|k'\rangle$ by a phase factor. The integer $I_{k'}$ has interchanged 00 and 11 sites from I_k. Their diagonal energies are equal in systems with *eh* symmetry. Their expansion coefficients in (9) thus satisfy $c_{k'}=\pm c_k$ and (21) merely states that diagrams with $n_p=0$ and 2 always occur in equally weighted pairs.

The spin density at site p in state ψ is

$$\rho_p=\langle\psi|2s_{pz}|\psi\rangle=\langle\psi|(a^\dagger_{p\alpha}a_{p\alpha}-a^\dagger_{p\beta}a_{p\beta})|\psi\rangle . \tag{22}$$

The ground-state expectation value is usually sought. We consider even N_e and a singlet ground state. Now ρ_p vanishes for each p since the operator in (22) annihilates any $|k\rangle$ with $n_p=0$ or 2 and generates a triplet diagram when $n_p=1$ that is orthogonal to all singlets in $\langle\psi|$. Systems with odd N_e and $S=\frac{1}{2}$ ground states, on the other hand, may show both positive and negative ρ_p. Polyene radicals[12,32] in Fig. 5(a), for example, with overall spin α have

$$\rho_{2p-1}>0,\quad p=1,2,\ldots,(N+1)/2$$
$$\rho_{2p}\leq 0,\quad p=1,2,\ldots,(N+1)/2\ . \tag{23}$$

In Hückel or SSH models with arbitrary nearest-neighbor t_p, the pairing theorem ensures $\rho_{2p}=0$ because the nonbonding MO has nodes at these sites. Correlations give $\rho_{2p}<0$ and a spin-density-wave (SDW) ground state. Magnetic resonance studies of odd-alternant radicals[40] and more recently of spins[41] in $(CH)_x$ indicate negative spin densities. Standard PPP parameters for $\delta=0.0$ radicals up to $N_e=N\leq 11$ overestimate[32] by $\sim 10\%$ the ratio $|\rho_-/\rho_+|$ of total negative and positive $(CH)_x$ spin densities.

Such considerations pose serious challenges for self-consistent schemes. HF theory readily accounts for vanishing ρ_p when N_e is even and all spins are paired in the lowest-energy MO's; but then $\rho_{2p}=0$ for odd N_e follows from the pairing theorem. The situation is reversed in unrestricted Hartree-Fock (UHF) theory,[42,43] which in Hubbard radicals gives both positive and negative ρ_p in a SDW ground state; but, S is not a good quantum number in UHF and SDW's are also found for even N_e. A heuristic compromise would be to use HF for even N_e, UHF for odd N_e. The latter could be calibrated against exact results in $N\sim 12$ systems and then applied to far larger N. Similar tests apply to CDW's or other symmetry-breaking solutions found self-consistently.

In addition to the representation of s_{pz} in (22), we have

$$s_p^+=a_{p\alpha}^\dagger a_{p\beta},\quad s_p^-=a_{p\beta}^\dagger a_{p\alpha}\ , \tag{24}$$

Static spin correlation functions like $\langle s_{pz}s_{qz}\rangle$ or $\langle \vec{s}_p\cdot\vec{s}_q\rangle$ may all be evaluated by considering their effects on $n_p=1$ sites in diagram $|k\rangle$. While the rules are more complicated, spin correlations in Hubbard or PPP models and fine-structure constants in triplet excited states open many new possibilities. Matrix elements over diagonal operators involving n_p are quite simple once the linear combination of VB diagrams has been normalized. Such charge correlation functions[44] are important for the electrostatic energies of partly ionic organic solids.

We turn next to the transition dipole of the lowest $\pi\rightarrow\pi^*$ excitation defining E_g, whose oscillator strength provides another comparison with experiment. The transition dipole from the ground (g) to excited (e) state is

$$\vec{M}=\langle e|\vec{\mu}|g\rangle\ , \tag{25}$$

where $\vec{\mu}$ is the dipole-moment operator. Spin is conserved but the eh and inversion indices change.[39] Table VIII lists transition dipoles for PPP polyenes, radicals, and ions whose geometries are given in Fig. 5 and transitions in Tables VI and VII. The reduced M_x from Hückel theory reflects the lower energy, and consequently higher weights, of adjacent C^+C^- sites in the correlated states. Reductions of $|M|^2$ of 2–3 from the Hückel value are observed[22] for $N\sim 6$–12 polyenes in solution. The agreement in Table VIII provides strong additional support for correlations, but more accurate gas-phase data is required for improved parametrization.

TABLE VIII. Transition moments M in Debye and oscillator strength per site f/N of the E_g excitations of N-site all-*trans* polyenes, radicals, ions, and cyanine dyes with standard molecular PPP parameters.

Length N	Alternation δ	Parallel M_x	Perpendicular M_y	Ratio[a] M^2/M^2 (Hückel)	f/N
Polyene					
6	0.07	6.965	2.137	0.4954	0.1694
8	0.07	8.405	2.225	0.4493	0.1635
10	0.07	9.681	2.327	0.4168	0.1592
12	0.07	10.838	2.423	0.3930	0.1560
Radical					
7	0.0	8.076	0.0	0.3883	0.1512
9	0.0	9.618	0.0	0.3453	0.1548
11	0.0	11.013	0.0	0.3110	0.1535
Ion					
7	0.0	10.062	0.0	0.6027	0.1536
9	0.0	12.409	0.0	0.5747	0.1521
11	0.0	14.706	0.0	0.5545	0.1499
Cyanine					
7	0.0	9.599	0.0	1.2355	0.1063
9	0.0	12.444	0.0	0.9773	0.1010
11	0.0	15.192	0.0	0.8848	0.0972

[a]Hückel value for same geometry and t_p.

The oscillator strength per site of nondegenerate transitions is[19]

$$f/N = 1.085\times 10^{-5}\nu\,|M|^2/e^2N\ , \tag{26}$$

where ν is the transition energy in cm^{-1} and M/e is in Å. The f/N results in Table VIII are surprisingly constant and may be extrapolated by inspection for alternating even polyenes, regular polyene radicals, or their ions. The results for correlated states are again quite different from the SSH enhancement of the midgap absorption by[45] $\pi^2\xi$ for a soliton half-width of $\xi\sim 7$. Both the energies and the intensities of in-gap excitations are qualitatively different for standard PPP parameters.

The π-bond order $P_{rs}^{(q)}$ between sites r and s in the correlated state q is[25]

$$2p_{rs}^{(q)} = \left\langle q \left| \sum_\sigma (a_{r\sigma}^\dagger a_{s\sigma} + a_{s\sigma}^\dagger a_{r\sigma}) \right| q \right\rangle\ , \tag{27}$$

and is the partial[46] of E_q with respect to t_r for adjacent sites. The evaluation of (27) is straightforward,[12] especially for $s=r+1$. The p_{rr+1} in the 2^1A_g state of even polyenes clearly indicate[25,12] two bond-alternation reversals, or two incipient neutral solitons, while odd segments have a single alternation crossover in the ground state.

The excited-state geometry may be found in general by readjusting the t_p according to $p_{p,p+1}$. The physical constraint of fixed overall length is usually included by keeping $\sum t_p$ constant. The solution of (1) gives a relaxed excited state and new bond orders. Test calculations[25] for standard π-electron parameters give small (<0.3 eV) relaxation energies and slight changes in $p_{r,r+1}$. The first iteration suffices for most applications. As shown by nonlinear spin-phonon coupling in soft lattices, however, different parametrizations may require several iterations for self-consistent bond orders.[47]

The bond orders (27) consequently provide a general method for geometry optimization of each electronic state $|q\rangle$ within the adiabatic or Born-Oppenheimer approximation. Nonlinear contributions to t_p, ϵ_p, U_p, or $V_{pp'}$ in (1) or anharmonic corrections to (17) are easily incorporated into the VB solution when the point-group symmetry is not lowered. Thus finite segments with C_2 symmetry are more useful than rings for studying distortions, and $N_e=N\leq 12$ chains afford many possible tests or comparisons. The restriction to the π-electron model (1) should be remembered, however, in view of the rich vibronic structure of finite even polyenes,[24] which clearly involve other modes besides C-C stretches.

VII. DISCUSSION

We have shown diagrammatic VB theory to give exactly the low-lying states of the quantum-cell model (1) for N_e, $N\leq 12$ chains and rings. Accurate extrapolations to $N\rightarrow\infty$ are possible, especially when different boundary conditions give decreasing and increasing sequences. The functional form for identifying critical exponents or vanishing energy gaps is less accurately found from finite systems. Ground-state energies per site, finite optical gaps, transition moments, spin densities, etc. all extrapolate smoothly and provide stringent tests for perturbation, mean-field, or renormalization calculations in one-dimensional models. For example, perturbation calculations[48] showing U to make slight modifications to the SSH results are sharply restricted to sufficiently small correlations that leave the Hückel states undisturbed and are at least an order of magnitude smaller than molecular PPP correlations. Self-consistent VB methods,[49] valence effective theories[50] or various extended HF schemes[29,42,43] offer improved descriptions of particular properties. Comparisons against numerical extrapolations are an important area for future work.

Quantum Monte Carlo methods[51] have recently been applied[52] to one-dimensional Hubbard models and extended Hubbard models with nearest-neighbor interaction V_1. They are in many respects complementary to VB theory. Monte Carlo methods yield the free energies, and thus the thermodynamics, of rather larger systems with $N\sim 20$—40; larger N, higher accuracy, and lower temperature are primarily questions of computer time. VB theory focuses instead on ground-state properties and excitation energies, since solving all eigenstates of large CI matrices is prohibitive. Exact $T=0$ results reflect directly small changes in the parameters; long-range interactions are readily included; and detailed analysis of the correlated state is possible. To be sure, smaller N in VB calculations requires longer extrapolation, thereby offsetting the greater accuracy.

Numerical approaches to infinite systems inevitably require extrapolation, and this topic merits additional attention. As suggested by the factorials in (3), direct solutions for ever larger N are not promising. The $\sim P_s/G$ symmetry-adapted linear combinations of VB diagrams cannot be reduced[12] further without approximation and cannot be stored more efficiently within a single integer i_k in (5). We encounter $P_s/G\sim 10^5$ in half-filled chains of 12, dimerized rings of 14, and quarter-filled rings of 16. For one ϕ_p per site the CI matrices increase by ~ 11 on adding two sites, which is only slightly less than 4^2 due to N_e and S conservation. Better extrapolation of *exact* results will consequently be restricted to a few additional points.

Approximate VB solutions allow more significant increases in N. In large-U Hubbard models the 2^N covalent states dominate in half-filled systems and lead to the effective Hamiltonian,[53]

$$\mathscr{H}_e = \sum_p 2J_p\,\vec{s}_p\cdot\vec{s}_{p+1}\ . \tag{28}$$

The antiferromagnetic exchange $J_p=2t_p^2/U$ describes virtual transfers in second-order perturbation theory and may be extended[54] in higher order. Now dimerized rings of $N\sim 26$ and chains of $N\sim 24$ are currently feasible with a VAX 11/780 computer. But the extreme simplification to (28) precludes any ionic states needed, for example, to define the optical gap.

The real-space VB basis allows intermediate choices for effective Hamiltonians, for example, based on an energy cutoff E'. Diagrams $|k\rangle$ with diagonal $E_k<E'$ in (1) are treated as before in constructing the matrix h_{kj} in (6). Transfers to diagrams $|q\rangle$ with $E_q>E'$, on the other hand, are considered to be virtual. In second order, we

have (28) with $J_p = 2t_p^2/(E_q - E_k)$ explicitly dependent on the diagonal energies. The resulting contribution is diagonal when t_p in (6) acts on connected singly occupied sites $p,p+1$ in $|k\rangle$ and off-diagonal for unconnected sites. We are testing such effective Hamiltonians when E' is chosen to retain approximately the lowest 5×10^4 symmetry-adapted diagrams, which in Hubbard or PPP models with $N_e = N = 18$ would easily include all covalent, singly ionic, and doubly ionic diagrams. Since the ground and low-lying states are only indirectly coupled to the neglected states, accurate solutions are expected for significantly larger N.

ACKNOWLEDGMENTS

We gratefully acknowledge support for this work through National Science Foundation Grant No. NSF-DMR-81-05010 and thank D. Nordlund for assistance with the VAX computer system.

[1]Z. G. Soos, Israel, J. Chem. 23, 37 (1983); Z. G. Soos and D. J. Klein, in *Molecular Association,* edited by R. Foster (Academic, New York, 1975), Vol. 1, pp. 1—119.
[2]O. J. Heilmann and E. H. Lieb, Trans. N.Y. Acad. Sci. 33, 116 (1971).
[3]H. Shiba and P. Pincus, Phys. Rev. B 5, 1966 (1972).
[4]K. Schulten, I. Ohmine, and M. Karplus, J. Chem. Phys. 64, 4422 (1976); for partial CI in $N \leq 12$ systems, see P. Tavan and K. Schulten, J. Chem. Phys. 72, 3547 (1980).
[5]S. Mazumdar and S. N. Dixit, Phys. Rev. Lett. 51, 292 (1983); S. N. Dixit and S. Mazumdar, Phys. Rev. B 29, 1824 (1984).
[6]J. C. Bonner and M. E. Fisher, Phys. Rev. 135, A640 (1964).
[7]E. H. Lieb and F. Y. Wu, Phys. Rev. Lett. 20, 1445 (1968).
[8]S. Ramasesha and Z. G. Soos, Solid State Commun. 46, 509 (1983).
[9]S. Ramasesha and Z. G. Soos, Synth. Met. (to be published).
[10]E. H. Lieb and D. C. Mattis, Phys. Rev. 125, 164 (1962), Appendix.
[11]S. Mazumdar and Z. G. Soos, Synth. Met. 1, 77 (1979).
[12]S. Ramasesha and Z. G. Soos, J. Chem. Phys. (to be published).
[13]S. Ramasesha and Z. G. Soos, Int. J. Quantum Chem. (to be published).
[14]S. R. Bondeson and Z. G. Soos, Phys. Rev. B 22, 1793 (1980).
[15]L. Pauling, J. Chem. Phys. 1, 280 (1933).
[16]E. R. Davidson, J. Comput. Phys. 17, 87 (1975); C. F. Bender and I. Shavitt, *ibid.* 6, 146 (1970).
[17]I. A. Musurkin and A. A. Ovchinnikov, Fiz. Tverd. Tela (Leningrad) 12, 2524 (1970) [Sov. Phys.—Solid State 12, 2013 (1971)].
[18]H. C. Longuet-Higgins and L. Salem, Proc. R. Soc. London, Ser. A 251, 172 (1959).
[19]L. Salem, *The Molecular Oribtal Theory of Conjugated Systems* (Benjamin, New York, 1966). See Chaps. 1, 3, 7, and 8 for extensive theoretical discussions of Hückel results and applications.
[20]Y. A. Bychkov, L. P. Gorkov, and I. E. Dzyaloshinskii, Zh. Eksp. Teor. Fiz. 50, 738 (1966) [Sov. Phys.—JETP 23, 489 (1966)].
[21]B. Roos and P. N. Skancke, Acta Chem. Scand. 21, 233 (1967).
[22]H. Suzuki, *Electronic Absorption Spectra and Geometry of Organic Molecules* (Academic, New York, 1967). See Chap. 8, 9, 11, 16, and 17 for detailed experimental and spectroscopic results.
[23]K. Ohno, Theor. Chim. Acta 2, 219 (1964).
[24]B. S. Hudson, B. E. Kohler, and K. Schulten, Excited States 6, 1 (1982) and references therein.
[25]L. R. Ducasse, T. E. Miller, and Z. G. Soos, J. Chem. Phys. 76, 4094 (1982); T. E. Miller, senior thesis, Princeton University, 1981 (unpublished).
[26]A. H. Zimmerman, R. Gygax, and J. I. Brauman, J. Am. Chem. Soc. 100, 5595 (1978).
[27]K. L. D'Amico, C. Manos, and R. L. Christensen, J. Am. Chem. Soc. 102, 1777 (1980).
[28]S. Etemad, A. J. Heeger, and A. G. McDiarmid, Ann. Rev. Phys. Chem. 33, 443 (1983) and references therein.
[29]M. Kertész, Adv. Quantum Chem. 15, 161 (1982); review of MO treatments of conjugated polymers.
[30]W. P. Su, J. R. Schrieffer, and A. J. Heeger, Phys. Rev. Lett. 44, 1698 (1979); Phys. Rev. B 22, 2099 (1980), and 28, 1138(E) (1983).
[31]Z. G. Soos and L. R. Ducasse, J. Chem. Phys. 78, 4092 (1983).
[32]Z. G. Soos and S. Ramasesha, Phys. Rev. Lett. 51, 2374 (1983).
[33]B. R. Weinberger, C. B. Roxlo, S. Etemad, G. L. Baker, and J. Orenstein (unpublished).
[34]G. V. Uimin and S. V. Fomichev, Zh. Eksp. Teor. Fiz. 63, 1894 (1972) [Sov. Phys.—JETP 36, 1001 (1973)].
[35]J. Orenstein and G. L. Baker, Phys. Rev. Lett. 49, 1042 (1982); C. V. Shank, R. Yen, R. L. Fork, J. Orenstein, and G. L. Baker, *ibid.* 49, 2660 (1982); J. Orenstein, Synthetic Metals II Conference, Los Alamos, 1983 (unpublished).
[36]O. Chalvet, J. Hoarau, J. Joussot-Dubien, and J. C. Rayez, J. Chem. Phys. 69, 630 (1972).
[37]A. D. McLachlan, Mol. Phys. 2, 276 (1959).
[38]J. Cizek, J. Paldus, and I. Hubac, Int. J. Quantum Chem. 8, 951 (1974).
[39]S. R. Bondeson and Z. G. Soos, Chem. Phys. 44, 403 (1979); J. Chem. Phys. 71, 3807 (1979); 73, 598 (1980).
[40]H. M. McConnell and D. B. Chesnut, J. Chem. Phys. 27, 984 (1957); H. M. McConnell and H. H. Dearman, *ibid.* 28, 51 (1958); M. W. Hanna, A. D. McLachlan, H. H. Dearman, and H. M. McConnell, *ibid.* 37, 361 (1962).
[41]H. Thomann, L. R. Dalton, Y. Tomkiewicz, N. S. Shiren, and T. C. Clarke, Phys. Rev. Lett. 55, 553 (1983); L. R. Dalton (private communication).
[42]K. R. Subbaswamy and M. Grabowski, Phys. Rev. B 24, 2168 (1981); J. C. Schug (private communication).
[43]H. Fukutome and M. Sasai, Prog. Theor. Phys. 67, 41 (1982).
[44]Z. G. Soos, L. R. Ducasse, and R. M. Metzger, J. Chem. Phys. 77, 3036 (1982).
[45]N. Suzuki, M. Ozaki, S. Etemad, A. J. Heeger, and A. G. McDiarmid, Phys. Rev. Lett. 45, 1209 (1980); A. Feldblum, J. H. Kaufman, S. Etemad, A. J. Heeger, T. C. Chung, and

A. G. McDiarmid, Phys. Rev. B 26, 815 (1982).
[46]C. A. Coulson, Proc. R. Soc. London, Ser. A 169, 413 (1939).
[47]S. Jagannathan and Z. G. Soos, J. Phys. Chem. 87, 4609 (1983).
[48]S. Kivelson and D. Heim, Phys. Rev. B 26, 4278 (1982).
[49]S. Kuwajima, J. Chem. Phys. 77, 1930 (1982).
[50]J. L. Bredas, R. R. Chance, R. Silbey, G. Nicolas, and Ph. Durand, J. Chem. Phys. 75, 255 (1981).
[51]M. Suzuki, Prog. Theor. Phys. 56, 1454 (1976); M. Suzuki, S. Miyashito, and A. Kuroda, *ibid.* 58, 1377 (1977); M. Barma and B. S. Shastry, Phys. Rev. B 18, 3351 (1978).
[52]J. E. Hirsch and D. J. Scalapino, Phys. Rev. Lett. 50, 1168 (1983); Phys. Rev. B 27, 7169 (1983); and (unpublished).
[53]J. H. Van Vleck, in *Quantum Theory of Atoms, Molecules, and the Solid State,* edited by P. O. Löwdin (Academic, New York, 1966), p. 475; P. W. Anderson, in *Solid State Physics,* edited by F. Seitz and D. Turnbull (Academic, New York, 1963), Vol. 14, p. 99.
[54]W. A. Seitz and D. J. Klein, Phys. Rev. B 9, 2159 (1974).